Science of the Total Environment 637–638 (2018) 1137–1149

Contents lists available at ScienceDirect

Science of the Total Environment

journal homepage: www.elsevier.com/locate/scitotenv

Photochemical model evaluation of 2013 California wild fire air quality impacts using surface, aircraft, and satellite data

K.R. Baker [a,*], M.C. Woody [a], L. Valin [a], J. Szykman [b], E.L. Yates [c], L.T. Iraci [c], H.D. Choi [d], A.J. Soja [d], S.N. Koplitz [a], L. Zhou [a], Pedro Campuzano-Jost [e], Jose L. Jimenez [e], J.W. Hair [f]

[a] U.S. Environmental Protection Agency, Research Triangle Park, NC, USA
[b] U.S. Environmental Protection Agency, Hampton, VA, USA
[c] NASA Ames Research Center, Moffett Field, CA, USA
[d] National Institute of Aerospace, NASA Langley Research Center, Hampton, VA, USA
[e] Department of Chemistry & Biochemistry, CIRES, University of Colorado, Boulder, CO, USA
[f] NASA Langley Research Center, Hampton, VA, USA

HIGHLIGHTS

- Rim fire plume well characterized by modeling system in horizontal and vertical space
- Predicted wildfire O_3 was overestimated at plume top and at the surface.
- Predicted wildfire $PM_{2.5}$ organic carbon underestimated at plume top.
- Elevated $PM_{2.5}$ from fire not always coincident with elevated O_3 at surface

GRAPHICAL ABSTRACT

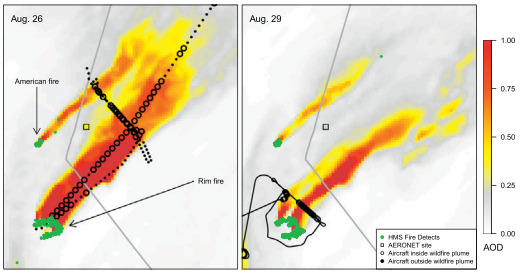

ARTICLE INFO

Article history:
Received 19 March 2018
Received in revised form 3 May 2018
Accepted 4 May 2018
Available online xxxx

Editor: Jianmin Chen

Keywords:
Wildfire
CMAQ
Ozone
$PM_{2.5}$
Lidar
AOD
SEAC4RS

ABSTRACT

The Rim Fire was one of the largest wildfires in California history, burning over 250,000 acres during August and September 2013 affecting air quality locally and regionally in the western U.S. Routine surface monitors, remotely sensed data, and aircraft based measurements were used to assess how well the Community Multiscale Air Quality (CMAQ) photochemical grid model applied at 4 and 12 km resolution represented regional plume transport and chemical evolution during this extreme wildland fire episode. Impacts were generally similar at both grid resolutions although notable differences were seen in some secondary pollutants (e.g., formaldehyde and peroxyacyl nitrate) near the Rim fire. The modeling system does well at capturing near-fire to regional scale smoke plume transport compared to remotely sensed aerosol optical depth (AOD) and aircraft transect measurements. Plume rise for the Rim fire was well characterized as the modeled plume top was consistent with remotely sensed data and the altitude of aircraft measurements, which were typically made at the top edge of the plume. Aircraft-based lidar suggests O_3 downwind in the Rim fire plume was vertically stratified and tended to be higher at the plume top, while CMAQ estimated a more uniformly mixed column of O_3. Predicted wildfire ozone (O_3) was overestimated both at the plume top and at nearby rural and urban surface monitors. Photolysis rates were well characterized by the model compared with aircraft measurements meaning aerosol attenuation was reasonably estimated and unlikely contributing to O_3 overestimates at the top of the plume. Organic carbon was underestimated close to the Rim fire compared to aircraft data, but was consistent with nearby surface measurements. Periods of elevated surface $PM_{2.5}$ at rural monitors near the Rim fire were not usually coincident with elevated O_3.

Published by Elsevier B.V.

* Corresponding author.
E-mail address: baker.kirk@epa.gov (K.R. Baker).

https://doi.org/10.1016/j.scitotenv.2018.05.048
0048-9697/Published by Elsevier B.V.

1. Introduction

Wildland fires are known to emit pollutants associated with negative health impacts in humans (Liu et al., 2015; Liu et al., 2016b; Rappold et al., 2011; Reid et al., 2016). Since wildfires are expected to increase in the future (Abatzoglou and Williams, 2016; Balch et al., 2017; Schoennagel et al., 2017), considerable interest exists to better relate wildland fire smoke with specific human health effects (Reid et al., 2016). Currently, estimation of human health impacts from wildfires relies on photochemical transport models, surface monitoring networks, and column-integrated, space-based measurements. Routine surface monitor networks, which are typically sparse in areas that historically have not exceeded the level of National Ambient Air Quality Standards, only capture a portion of the spatial extent of wildland fire smoke plumes (Reid et al., 2016). Satellite products provide broad spatial coverage especially when aggregated over time, but do not explicitly provide short-term (e.g., sub-annual) surface level estimates of either particulate matter less than 2.5 μm ($PM_{2.5}$) or ozone (O_3) (Zoogman et al., 2014). Efforts have been made to infer long-term surface $PM_{2.5}$ from satellite data (Boys et al., 2014; Van Donkelaar et al., 2006) but these approaches are often paired with other information like surface monitors and model output (Van Donkelaar et al., 2016). Previous work also shows that only using remotely sensed data can result in underestimated aerosol emissions for specific fires (Saide et al., 2015). In addition, remotely sensed data have limited and sometimes no spatial coverage for small fires (Hao and Larkin, 2014), large fires with pyrocumulus, in the presence of clouds and in areas with high surface reflectivity such as parts of the western United States (Loría-Salazar et al., 2016; Saide et al., 2015).

Photochemical grid models have been applied in the past to estimate the impacts of wildland fires in aggregate (Cai et al., 2016; Fann et al., 2013; McKeen et al., 2002) and also for specific fires (Baker et al., 2016; Yu et al., 2016; Zhou et al., 2018) and have the advantage of providing hourly surface level estimates of O_3 and $PM_{2.5}$ at a temporal and spatial resolution typically better than satellite retrievals and without the gaps of the surface monitor network. Further, photochemical transport models can be used for source attribution to differentiate the impacts of specific fires or groups of fires from other sources (e.g., anthropogenic and biogenic) to modeled primary and secondary pollutants (Kwok et al., 2015; Kwok et al., 2013). Surface monitoring networks provide valuable measurements to supplement air quality forecasts (Al-Saadi et al., 2005) and assess model performance and forecasting skill (Kondragunta et al., 2008).

Photochemical grid modeling systems estimate both $PM_{2.5}$ and O_3 from wildland fires (Baker et al., 2016), but model skill in replicating emissions, plume transport, and complex chemical evolution is critically important to provide confidence that pollutant estimates attributed to wildland fire are not systematically biased when matched with health effect data (Baker et al., 2016; Liu et al., 2016a; Zhou et al., 2018). Wildfire emissions estimation approaches have evolved (Wagstrom et al., 2014), but can vary by orders of magnitude (Al-Saadi et al., 2008; Larkin et al., 2010; Reid et al., 2009; Rolph et al., 2009). The fire plume rise along with local-to-synoptic scale meteorology impacts plume transport (Peterson et al., 2015) and also influences the rate of secondary pollutant formation (Bian et al., 2017; Sakamoto et al., 2016). Model misplacement of smoke plumes could result in incorrect population exposure estimates and biases in vertical and horizontal plume extent could lead to systematic over or under-estimates of $PM_{2.5}$ and ozone through error in dilution. The entirety of the wildfire emission estimates and model transport errors can result in incorrect population exposure estimates.

The 2013 Rim fire in the central Sierra Nevada mountains was one of the largest wildfires on record in California. The progression of the fire and the associated smoke plumes were observed by a combination of systems including existing air quality surface monitoring networks, satellite instruments, and a suite of special-study aircraft measurements providing detailed chemical composition information (Peterson et al., 2015; Toon et al., 2016; Yates et al., 2016). The size of this fire and availability of surface and aloft measurements make this an ideal case for model evaluation of wildfire smoke transport and chemical evolution. Here, the Community Multiscale Air Quality (CMAQ) model using meteorological input from the Weather Research and Forecasting (WRF) model and wildland fire emissions estimates from the SmartFire2/BlueSky framework (Larkin et al., 2010) was applied at 4 and 12 km grid resolution isolating the impacts from wildland fires using emission perturbation sensitivity simulations. These impacts are compared with surface, aircraft, and space-based observations to evaluate horizontal and vertical plume placement and plume chemical evolution.

Aircraft measurements from the Studies of Emissions and Atmospheric Composition, Clouds and Climate Coupling by Regional Surveys (SEAC4RS) (Toon et al., 2016) and the Alpha Jet Atmospheric eXperiment (AJAX) (Yates et al., 2016) were used to determine how well CMAQ replicates complex gas phase chemical reactions leading to O_3 formation and also provide some information about how well the modeling system captures $PM_{2.5}$ and plume placement. Data from rural ground monitoring stations were used to evaluate CMAQ simulations of surface O_3 and $PM_{2.5}$. Ambient surface measurements taken in Reno, NV were used to understand Rim fire impacts in a downwind urban area. These comparisons between model estimates, surface monitors, and satellite based estimates also illustrate the strengths and weaknesses of each type of information toward informing wildland fire related human exposure assessments.

2. Methods

2.1. Modeling system overview

The CMAQ version 5.2 model was applied with ISORROPIA II inorganic thermodynamics (Fountoukis and Nenes, 2007), aqueous phase chemistry (Fahey et al., 2017), and gas phase chemistry based on the Carbon Bond 6 revision 3 mechanism (Emery et al., 2015). Primary organic aerosol is treated as non-volatile and secondary organic aerosol (SOA) is formed based on yields from precursor gases including toluene, xylenes, benzene, isoprene, monoterpenes, and sesquiterpenes. SOA is aged based on oligomerization toward a non-volatile form (Carlton et al., 2010). This treatment conserves the POA mass and results in low SOA/POA ratios, which is consistent with most observations of ambient fire plumes, albeit the aging of the OA in the plumes is not captured (Cubison et al., 2011; Shrivastava et al., 2017). The ratio of organic mass to organic carbon is assumed to be 1.7 for wildland fire emissions (Simon and Bhave, 2012). All modeled aerosol species have a refractive index for photolysis attenuation. Elemental carbon is mapped to black carbon and organic aerosol species are mapped to dust because brown carbon is not part of the refractive index in CMAQ. Photolysis rates were attenuated in the presence of model predicted particulate matter (Baker et al., 2016).

Meteorological inputs to CMAQ were simulated with the WRF model version 3.8 (Skamarock et al., 2008). Both models were applied for the entire year of 2013 for a 12 km domain covering the contiguous U.S. and from August 1 to September 15, 2013 to match the period of the Rim fire for a smaller 4 km domain (Fig. S-1) covering northern California and Nevada. Each model used 35 layers to represent the vertical atmosphere from the surface up to 50 mb. This WRF configuration has performed well for surface temperature, wind fields, and mixing layer height in California (Baker et al., 2013) and the Pacific Northwest (Zhou et al., 2018). The modeling system was applied with and without wildland fire emissions to estimate how air quality would change in the absence of all wildland fire emissions for the time period field measurements were made and Rim fire burning was most intense.

WRF was initialized with the 12 km North American Mesoscale (NAM) analysis product and CMAQ was initialized with a global model simulation (GEOS-Chem) which provided initial chemical

conditions and also boundary inflow into the larger 12 km contiguous U.S. CMAQ simulation (Henderson et al., 2014). Initial and boundary conditions for the smaller 4 km domain were extracted from the larger 12 km simulation. Anthropogenic emissions were based on the 2011 National Emission Inventory with 2013 specific data used for point sources reporting continuous emissions data. Biogenic emissions were estimated with the Biogenic Emission Inventory System version 3.6, which has been shown to perform well for biogenic VOC in central California and the Sierra Nevada foothills regions (Bash et al., 2015).

Daily fire location and burn area for wild and prescribed fire was estimated using the SmartFire2 system, which is largely based on satellite products (Raffuse et al., 2009). Location, burn area, and date information is provided to the BlueSky framework to estimate fuel type, fuel moisture, and fuel consumption that is used to estimate daily emissions of CO, NO_X, VOC, SO_2, NH_3, and $PM_{2.5}$. Daily emissions for the Rim fire are shown in Table S-1 and by fuel type in Table S-2. Average emission factors by fuel type are shown in Table S-3. Emission factors varied by fuel type but not day-to-day. Fuel specific CO emission factors are somewhat higher than inferred from measurements for this particular fire (Yates et al., 2016) but generally consistent with other published values (Simpson et al., 2011; Urbanski, 2013). The Sparse Matrix Operator Kernel Emissions (SMOKE) model (https://www.cmascenter.org/smoke/) applied a generic temporal profile for wildfire to allocate daily emissions to hour of the day (Fig. S-2) and also applied speciation profiles to generate compound specific emissions from NO_X, VOC, and $PM_{2.5}$ (Table S-4). These chemical speciation profiles were used for each fire and not specific to fuel type or combustion phase.

2.2. Model estimates of AOD

CMAQ employs two approaches to estimate aerosol optical depth (AOD or τ). One approach calculates AOD with reconstructed extinction values from the Interagency Monitoring of Protected Visual Environments (IMPROVE) monitoring network (Pitchford et al., 2007). The second approach estimates AOD based on scattering and absorption coefficients using approximations to Mie scattering theory (Binkowski et al., 2007), which is used to solve the radiative transfer equation for calculating photolysis rates in the photochemical mechanism. The reconstruction extinction method represents an AOD at $\lambda = 550$ nm, consistent with the Moderate Resolution Imaging Spectroradiometer (MODIS) AOD data products used in the analysis. The Mie based approach is calculated at multiple wavelengths, with the closest to AOD wavelengths being 381 and 607 nm. Therefore, the Mie based AOD (τ) is extrapolated to 550 nm based on the spectral dependence of AOD (Eq. (1)) with the Angstrom exponent (α) determined from Eq. (2).

$$\tau_{550} = \tau_{381}\left[\frac{550}{381}\right]^{-\alpha} \quad (1)$$

$$\alpha = -\frac{log\frac{\tau_{381}}{\tau_{607}}}{log\frac{381}{607}} \quad (2)$$

Modeled AOD at 550 nm using the reconstructed light extinction approach compares well with Mie scattering theory ($r^2 = 0.986$; slope = 1.18; intercept = −0.01) but tends to be slightly higher for AOD values greater than 3 for this modeling period and region focused on the Rim fire (Fig. S-3).

2.3. Remotely sensed data

Aerosol optical depth from MODIS (Kaufman et al., 1997; Tanré et al., 1997) aboard the Terra and Aqua satellite (3 and 10 km resolution data products) (Levy et al., 2013; Munchak et al., 2013) were used to evaluate large-scale transport and the horizontal extent of the Rim fire plume. The 10 km spatial resolution product was regridded to the 12 km model domain, while the 3 km AOD product was regridded to both the 4 and 12 km domains. A qualitative assessment of smoke plume horizontal extent is also possible using satellite RGB (visible) imagery from the MODIS or other satellite instruments capable of producing high quality visible images to identify smoke from other visible features like clouds or artifacts such as sub glint. This type of imagery is available via NASA Worldview products. Visual images from MODIS were used to qualitatively assess downwind horizontal plume extent (https://worldview.earthdata.nasa.gov/).

MODIS Collection 6 Level 2 AOD from Terra and Aqua (C6_MOD04/MYD04_L2) was downloaded using the EPA Remote Sensing Information Gateway (https://www.epa.gov/hesc/remote-sensing-information-gateway). The RSIG provides a direct connection to the current MODIS archive for several atmospheric products at Goddard Space Flight Center and allows for automated regridding of MODIS AOD to match the grid used for CMAQ in this analysis. The estimated error for the C6 land AOD product is $\pm 0.05\,\tau + 15\%$ at 550 nm, which is a global error estimate that varies regionally and seasonally. Remotely sensed AOD products may be limited or provide no information in the presence of clouds, areas with high surface reflectivity, very large fires with pyrocumulus (Loría-Salazar et al., 2016), and small fires (Hao and Larkin, 2014). The Terra and Aqua data sets were not aggregated temporally. The sun-synchronous orbit of Terra results in data provided at approximately 10:30 am local time and Aqua at 1:30 pm local time. Surface based level 1 AOD measurements from the Aerosol Robotic Network (AERONET; aeronet.gsfc.nasa.gov) monitors that were in proximity to the Rim fire during August 2013 were used to supplement space-based AOD products.

Cloud-Aerosol Lidar with Orthogonal Polarization (CALIOP) onboard the Cloud-Aerosol Lidar and Infrared Pathfinder Satellite Observations (CALIPSO) satellite is a space-based lidar instrument that detects the vertical distribution of clouds and atmospheric aerosols (Omar et al., 2009). A smoke-plume injection-height product is produced by extracting smoke-laden aerosols from CALIOP vertical data. Smoke is verified using visible imagery and overlaying CALIPSO tracks. Smoke-laden air parcels, extracted at 100 m vertical and 1-second horizontal intervals along the CALIPSO track, were used to initialize the Langley Trajectory Model (LaTM). Modern-era Retrospective Analysis for Research and Applications, version 2 (MERRA-2) hourly re-analysis meteorological data were input to LaTM simulations (Molod et al., 2015). Smoke-laden aerosols are tracked back in space and time (15-minute time step) until vertically and horizontally coincident (within 20 km) with daily MODIS fire detections. Multiple CALIOP tracks were used to determine daily smoke plume injection height and detrainment (Soja et al., 2012), however for certain days and fires there may not be available CALIPSO tracks crossing smoke plumes.

Modeled plume top is estimated using a threshold approach where the plume top is defined as the height where modeled CO from wildfire first exceeds a nominal threshold of 20 ppb when starting at the model top and going toward the surface (Sicard et al., 2006).

2.4. Airborne and surface measurements

Airborne measurements were from multiple field campaigns. The NASA-AJAX mission collected O_3 on August 29, 2013 downwind of the Rim fire (Yates et al., 2016). A highly instrumented airborne platform (NASA DC-8, SEAC4RS campaign) (Toon et al., 2016) sampled in the Rim fire plume on August 26, 2013 making a long transect through the center of the Rim fire plume after several horizontal transects. Transects were made further downwind of the Rim fire sometimes include impacts from both the Rim fire and other fires in the Pacific Northwest (Forrister et al., 2015; Liu et al., 2017). Aircraft measurements of CO, CO_2, NO, NO_2, HNO_3, PAN, CH_2O, O_3, speciated PM_1 (DeCarlo et al., 2006; Dunlea et al., 2009), and photolysis rates (Fisher et al., 2016; Toon et al., 2016) were matched with modeled estimates in time and

space at the closest modeled hour and using the grid cell where the aircraft was located at the time of the measurement. Each of these measured chemical species were adjusted for background by subtracting the median flight-day value. The August 26 DC-8 flight included a Differential Absorption Lidar (DIAL) - High Spectral Resolution Lidar instrument (HSRL) (Hair et al., 2008) that provides aerosol backscatter, extinction, depolarization, and O_3 profiles that can be used to evaluate the wildfire plume vertical and horizontal structure.

Model estimates are compared to hourly surface O_3 measurements from the Clean Air Status and Trends Network (CASTNET) and daily averaged speciated $PM_{2.5}$ from the IMPROVE (http://vista.cira.colostate.edu/Improve/) network. Modeled $PM_{2.5}$ organic aerosol was adjusted to organic carbon using OC:OM ratios for specific secondary organic aerosol groups and did not include primarily emitted mass associated with organics (PNCOM). Model performance is also compared to a suite of measurements collected at the Reno, NV NCore station (https://www3.epa.gov/ttnamti1/ncore.html), including CO, NO_Y, O_3, and $PM_{2.5}$. Surface monitor data were paired with surface model estimates by hour and in space by matching the model estimate from the grid cell where the monitor was located.

3. Results

Smoke from the Rim fire and other fires in the western U.S. were visible from space and discernible in remotely sensed data products from multiple satellites. Analysis spans the entire period of the Rim fire, but plume extent assessments are focused on Aug. 25, 26 and 29 due to available remotely sensed data and aircraft transects flown through sections of the Rim fire smoke plume, which provides information about how well the model estimated plume placement and chemical evolution. Routine monitor network data are also included to provide information about surface level chemical impacts represented by the modeling system. Table 1 shows which components of the modeling system were compared with satellite, aircraft, and routine surface measurements. Daily maps of wildfire smoke from the Rim fire and other nearby fires are shown along with NO_2 and formaldehyde retrievals from the OMI satellite in supporting information. These daily maps of smoke plumes show the day to day variability in plume direction. The daily OMI NO_2 and formaldehyde retrievals only occasionally show well-formed high levels of these pollutants in the vicinity of the Rim fire with many of the days providing little or no relevant information. Regional warm temperatures and dry air was well characterized (Fig. S-4) while surface level winds were over-estimated by WRF in portions of the Sierra Nevada (Fig. S-5) although regional flows were well characterized as described below.

3.1. Plume transport - horizontal

Model (4 km) estimated and MODIS AOD (3 and 10 km) are shown for 21 UTC on Aug 26 and 29 in Fig. 1. Fig. 2 shows 12 km model and 10 km MODIS for August 25 over a larger area of the Pacific Northwest. Areas with elevated AOD are largely related to the plume downwind of the Rim fire and American fire (CAL FIRE, 2013), a smaller fire located north of the Rim fire. While quantitative comparison of modeled and satellite AOD is complicated by the presence of clouds near the Rim fire and large surface reflectance east of the Sierra Nevada (Loría-Salazar et al., 2016), the modeling system does well at predicting the orientation and extent of the Rim fire plume on both days indicating that the space-based measurements have value in diagnosing column-integrated smoke transport of large wildfire plumes (Figs. 1 and 2). However, this comparison highlights the challenges associated with using satellite products to show wildland fire impacts because large fires may not be fully characterized as part of the AOD analysis as the densest portion of the Rim fire plume is not evident in the satellite AOD product. Further, it is important to keep in mind that both the MODIS AOD and visible smoke images from MODIS do not provide a

Table 1
List of model comparison with satellite, aircraft, and routine surface measurements by spatial extent of the smoke plume, vertical plume profile, plume top, and surface. For each combination the corresponding Figures are shown to facilitate navigation of the presented model performance evaluation.

Type of Evaluation	Model	Satellite	Aircraft	Routine surface	Figures
Spatial extent of plume	AOD	MODIS AOD, Visible image		AOD	Figs. 1, 2
Vertical plume profile	OH				Fig. S13
Vertical plume profile	SO_2, NH_3				Fig. S12
Vertical plume profile			Aerosol backscatter and O_3		Fig. S8
Plume top	CO and O_3		CO and O_3		Figs. 3, 4, S-6
Plume top	NO_X, PANs, nitric acid, formaldehyde, $PM_{2.5}$ organic aerosol		NO_X, PANs, nitric acid, formaldehyde, PM_1 organic aerosol		Fig. 4
Plume top	Plume top	CALIPSO / trajectory plume top			Fig. S7
Plume top	Photolysis rates		Photolysis rates		Figs. 3, 4
Plume top	NO_X, PANs, formaldehyde, acetaldehyde		NO_X, PANs, formaldehyde, acetaldehyde		Fig. S9
Plume top	$PM_{2.5}$ sulfate ion, nitrate ion, ammonium ion, organic aerosol		PM_1 sulfate ion, nitrate ion, ammonium ion, organic aerosol		Fig. S11
Plume top	Temperature		Temperature		Fig. S10
Surface	$PM_{2.5}$ organic carbon			$PM_{2.5}$ organic carbon	Fig. 6
Surface	Total $PM_{2.5}$			Total $PM_{2.5}$	Fig. 8
Surface	O_3			O_3	Figs. 5, 8
Surface	$PM_{2.5}$ elemental carbon			$PM_{2.5}$ elemental carbon	Fig. S14
Surface	$PM_{2.5}$ nitrate ion			$PM_{2.5}$ nitrate ion	Fig. S15
Surface	$PM_{2.5}$ sulfate ion			$PM_{2.5}$ sulfate ion	Fig. S16
Surface	NO_X, NO_Z			NO_X, NO_Z	Fig. S17
Surface	Temperature, water mixing ratio, wind speed, wind vector error			Temperature, water mixing ratio, wind speed, wind vector error	Fig. S4, S5

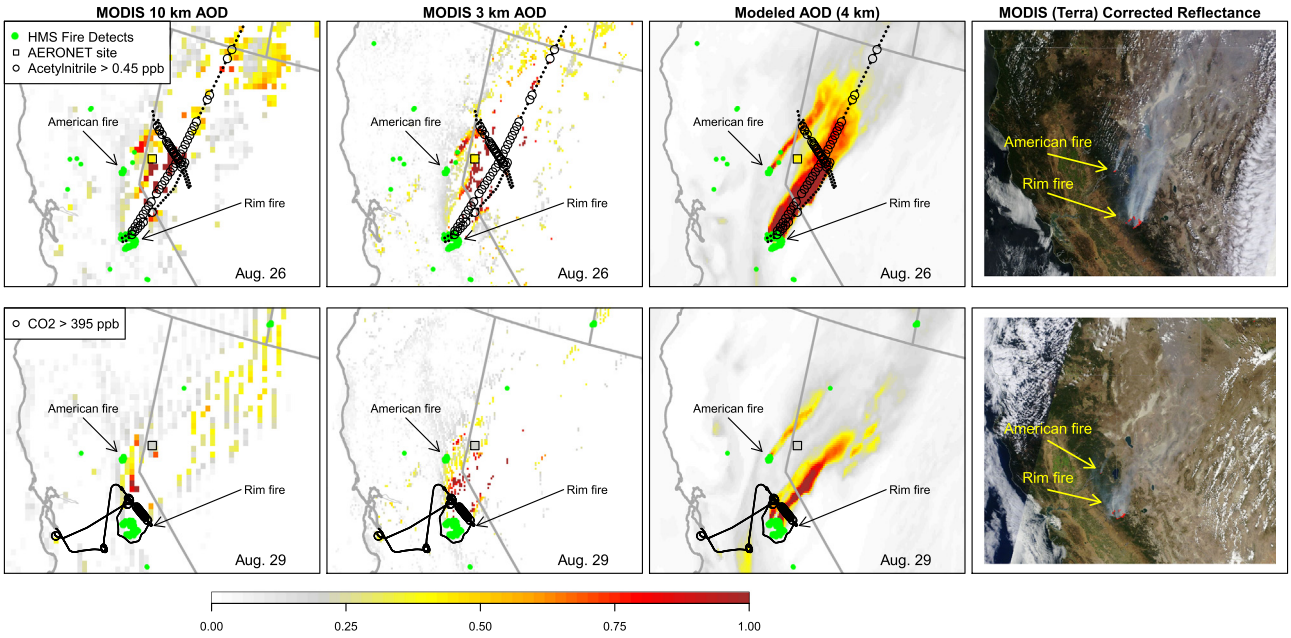

Fig. 1. MODIS aerosol optical depth at 3 and 10 km resolution on August 26 (top row) and August 29 (bottom row), 2013 at 21 UTC. Modeled AOD at 4 km resolution. Warmer colors indicate the presence of aerosols, most notably for the Rim and American wildfires in east-central California. The largest aerosol concentrations in the downwind plume from the Rim fire are not part of the satellite AOD product due to the MODIS cloud filtering algorithm but are captured in the corrected reflectance true color images. Larger open symbols show aircraft transects in wildfire plume based on chemical measurements and small dots indicate aircraft positions outside wildfire plumes. (For interpretation of the references to color in this figure legend, the reader is referred to the web version of this article.)

quantitative estimate of O_3 or $PM_{2.5}$ at the surface as the smoke plume may be well above the surface when seen by satellites.

On August 25th, the Rim fire had been burning for several days and a smoke plume is evident in both MODIS AOD and the visible true color image from east-central California downwind to western Idaho, northern Montana, and southern Canada (Fig. 2). The model simulates a very similar pattern of AOD and often captures magnitude in closer proximity to the fire compared to MODIS and AERONET AOD, again indicating that the modeling system does well at capturing the local to continental scale transport for this fire. Further downwind of the Rim fire, modeled AOD patterns are similar to remotely sensed data but generally lower. The model underestimated AOD compared to the closest AERONET site in Reno (mean bias of −0.1; mean error of 0.4; normalized mean bias of −24%; normalized mean error of 102%), especially when observed AOD is elevated (mean bias of −0.5; mean error of 0.8; normalized mean bias of −51%; normalized mean error of 74%). Modeled AOD tends to be lower than measured at AERONET sites in Idaho and Montana during this period. The good agreement of smoke plume placement is largely due to the WRF model appropriately capturing local to regional scale wind patterns. Winds during this period were generally out of the south and southwest due to a broad ridge over the southern plains forcing air flow around it. The model captures these large-scale wind flows based on good agreement with modeled plume orientation and remotely sensed smoke and also based on surface level model performance (Fig. S-5).

Plume transects were made downwind of the Rim fire as part of the SEAC4RS and AJAX field campaigns and are shown in Fig. 1 with large open circles when chemical measurements indicated the aircraft was inside a wildfire plume. The horizontal extent of wildfire plumes was generally similar between the aircraft and satellite AOD but a direct comparison is challenging due to the lack of satellite data for the Rim fire on that day. The model and aircraft plumes compare very well downwind of both the Rim and American fires on August 26. The MODIS AOD retrieval and visible imagery (Fig. 1), however, both indicate that the plume is slightly wider than suggested by aircraft transects

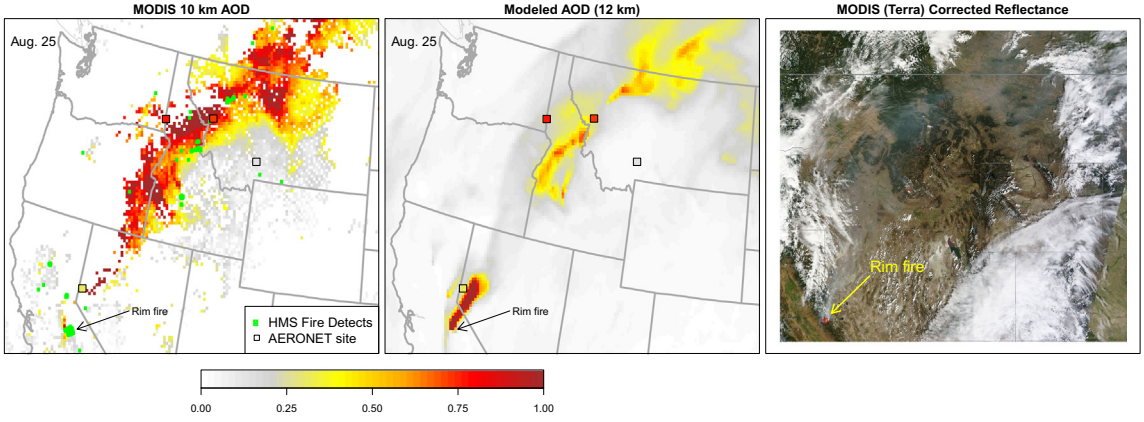

Fig. 2. MODIS aerosol optical depth at 10 km resolution on August 25, 2013 at 18 UTC. CMAQ 12 km modeled AOD and visible smoke are also shown. Warmer colors indicate the presence of aerosols. (For interpretation of the references to color in this figure legend, the reader is referred to the web version of this article.)

on August 26. This discrepancy on August 26 may be due to the aircraft transects not completely capturing the full vertically-integrated horizontal extent of the plume. On August 29, the aircraft and satellite plume width compare well but the modeled plume is notably less wide near the fire. Overall, the horizontal extent of the Rim fire plume compared well between aircraft and satellite products with the model

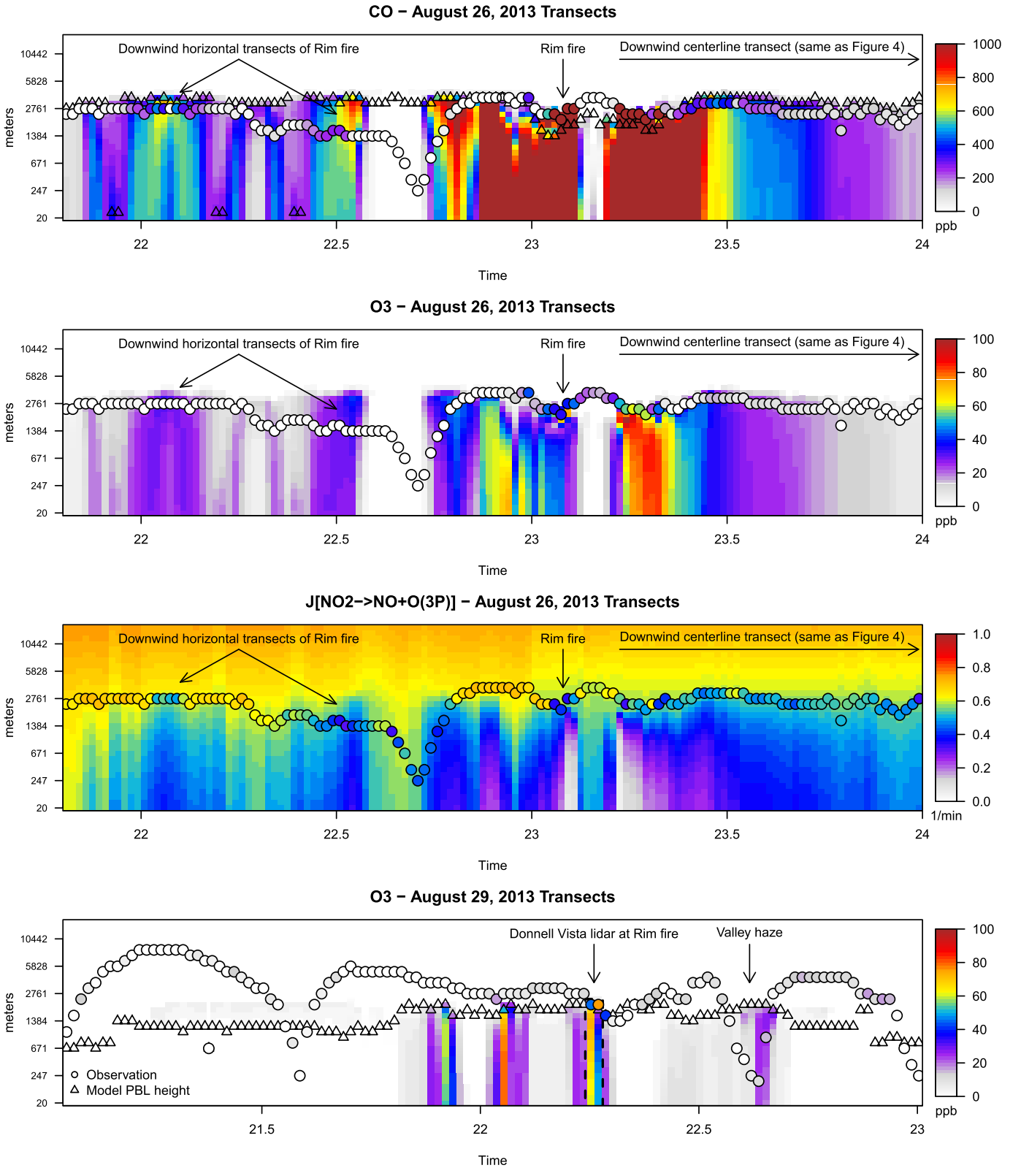

Fig. 3. Aircraft measurements (circles) compared with column model predictions of photolysis rates, CO and O_3 on August 26, 2013 and O_3 on August 29, 2013. The dashed box outline on the August 29 panel (bottom panel) indicates the Rim fire plume top and bottom, which was well mixed throughout the plume, as determined by ground based lidar (Yates et al., 2016). Both model and measurements of CO and O_3 have been adjusted to remove background and reflect only wildfire contribution. Modeled surface layer mixing height is also shown (triangles).

showing good agreement although the modeled plume may at times be slightly narrower than observed.

3.2. Plume transport – vertical

An estimate of plume top can be inferred from aircraft altitudes during smoke plume transects made on August 26 (SEAC4RS) and August 29 (AJAX) since these aircraft were generally flown at the top of plumes to capture smoke impacts while maximizing crew safety. Fig. 3 shows aircraft measurements compared with modeled surface mixing layer height (PBL height) and column estimates of CO, O_3, and NO_2 photolysis rates for flights near the Rim fire. All ambient points are shown to illustrate the flight path and show when measured values approach zero, which may indicate chemical destruction (i.e., for O_3) or that the aircraft was not in the fire plume. The same comparison of aircraft chemical measurements and modeled plume are shown in Fig. S-6 to show chemical structure horizontally across the plume with measured acetylnitrile plotted as an additional indicator about whether the aircraft was in the smoke plume.

A land-based lidar at Donnell Vista (Yates et al., 2016) measuring plume vertical extent supports using the aircraft altitude during transects as an approximation of plume height. The lidar estimated a similar plume height as the altitude of the Alpha Jet where both were coincident in time and space on August 29 (Fig. 3). The plume top estimated by the modeling system for both August 26 and 29 compares well with the altitude of the aircraft making smoke plume measurements and also with lidar estimates on August 29 (Fig. 3). On the 26th, the modeled plume top extends above the modeled boundary layer at the Rim fire but otherwise tends to be within the surface mixing layer with occasional sheer and decoupling between free troposphere and surface mixing layer (shown on August 29 flight during approach to the Rim fire). The daily distribution of model estimated plume top is paired with CALIPSO-based estimates in Fig. S-7. These distributions reflect both diurnal variability and spatial variability near the Rim fire. In general, the modeled distribution of smoke plume top compares well with those based on back trajectories from CALIPSO overpasses downwind of the Rim fire.

Surface lidar measurements at Donnell Vista, CA (Yates et al., 2016) in the afternoon of August 29 suggest that emissions were well mixed from the surface to plume top. The aircraft DIAL aerosol backscatter retrieval shows that aerosols were well mixed from the surface to plume top downwind of the fire. However, the DIAL O_3 profile retrieval suggests O_3 tends to be enhanced at the plume top during the August 26 flight and is consistent with the in-situ measurements of O_3 on the aircraft slightly earlier (15 min) (Fig. S-8). The modeling system shows a well-mixed plume (CO and primary organic aerosol) from the surface to a plume height that is consistent with aerosol backscatter profiles retrieved by DIAL on August 26. The model predicts O_3 enhancement at the top of the plume in very close proximity to the Rim fire then becomes well mixed through the surface mixing layer downwind. Aircraft platform measured photolysis rates at the plume top compare well with modeled values (Fig. 3), but measurements are not available to understand vertical variability in photolysis rates in the smoke plume. The well-mixed O_3 estimated by the modeling system is not consistent with the aircraft DIAL profile, which suggests stratified layers of O_3 enhancement. The lack of stratification in CMAQ may be related to excessive vertical mixing or underestimated photolysis attenuation within the boundary layer resulting in over-stated photochemistry.

3.3. Smoke plume – chemical evolution

Fig. 4 shows plume top measurements and model estimates (4 and 12 km) during the final downwind transect of the Rim fire on August 26. Both are shown as a function of time and the entire transect shown here covers approximately 19 h (500 km distance and mean wind speed of ~7.5 m/s) of plume age. Primary and secondarily formed pollutants are highest when the plume is fresh and decrease as the plume ages. Modeled carbon monoxide (CO) tends to be higher than measured near the fire and does not decrease as rapidly as the ambient data, which is generally consistent with the CO emission factors used here being higher than inferred from August 26 aircraft measurements (Yates et al., 2016). Similarly, modeled O_3 is higher than aircraft measurements near the fire and does not decrease as rapidly downwind (Fig. 4). NO_X is well predicted by the modeling system both near the fire and downwind (Fig. 4).

CO is often used as an indicator of plume dilution given slow reactivity and long atmospheric lifetime compared to other pollutants. The observed O_3/CO ratio suggests O_3 production outpaces plume dilution both near the source and further downwind at 10 to 15 h of plume age before production becomes minimal. Modeled O_3 enhancements stay consistent downwind while the observed ratio shows periodic departures from the more consistent trajectory. Observed and modeled NO_X/CO ratios are similar near the fire but an enhancement in the ambient ratio downwind that is generally consistent with an observed O_3/CO enhancement is not captured. The model does well at capturing aircraft NO_2 photolysis rate measurements (Fig. 4), which suggests model representation of aerosol attenuation of photolysis rates is not contributing to degraded O_3 performance in the top edge of the plume.

As noted in the previous section, aircraft LIDAR data (Fig. S-8) suggest stratified O_3 formation that is enhanced at the top of the Rim fire plume on August 26 but the modeling system estimated O_3 mixed through the entire vertical column and for too long of a time period as the plume moved downwind. Photolysis rates are well characterized at the plume top but no information is available about the rest of the column (Fig. 3) to better understand how inconsistencies between the surface and plume top may translate into O_3 over-estimates. Modeled photolysis rates decrease rapidly toward the surface in proximity to the fire with reductions up to approximately 50% where aerosol concentrations are highest. Previous work applying more aggressive photolysis attenuation in the presence of aerosol resulted in less O_3 formation in smoke plumes but did not eliminate over-predictions at surface monitor locations (Baker et al., 2016). As discussed in subsequent sections, downwind surface O_3 is similarly over-estimated as at the plume top for this study. Column measurements of meteorology, chemical species, and physical properties such as photolysis rates are needed to better understand the complex chemical and physical processes governing vertically heterogeneous O_3 levels in the plumes of large wild fire.

The lack of nitric acid and presence of peroxyacteyl nitrates (PANs) in the fire plume (Figs. 4; S-9) suggest highly reactive VOC emitted by the fire (e.g., aldehydes) are being rapidly converted to peroxacyl radicals, which react with NO_2 to form PAN (and similar compounds). This smoke plume O_3 production process has been demonstrated for another large wild fire using this modeling system (Baker et al., 2016) and observed in other wildfire smoke plumes in California (Cai et al., 2016). The model does not predict HNO_3 formation in the plume consistent with ambient measurements, but does tend to over-estimate PAN which may be the result of near-fire over-estimation of acetaldehyde (Fig. S-9). The model does well at capturing plume top (Fig. S-10) and surface (Fig. S-3) temperature which is likely not a factor in PAN performance. The VOC speciation profile may be attributing too much of the VOC emissions to formaldehyde and acetaldehyde or the profile may be biased and already include rapidly produced secondary VOC. Further, over-estimated total VOC emissions could result in too much formaldehyde and acetaldehyde emitted into the modeling system.

CMAQ under-estimates the near-fire peak in organic aerosol, simulating only a third of observed levels and estimates a flat OA/CO ratio of ~0.05 while the observed OA/CO ratio varies significantly and exceeds 0.2 for the first half of the downwind transect. Other studies have shown that grid resolution has large impacts on near-source model prediction of primary pollutants (Baker et al., 2014). Given the grid resolution used here, the model would likely under-estimate primary pollutants at the fire and have less impact downwind as the plume becomes more

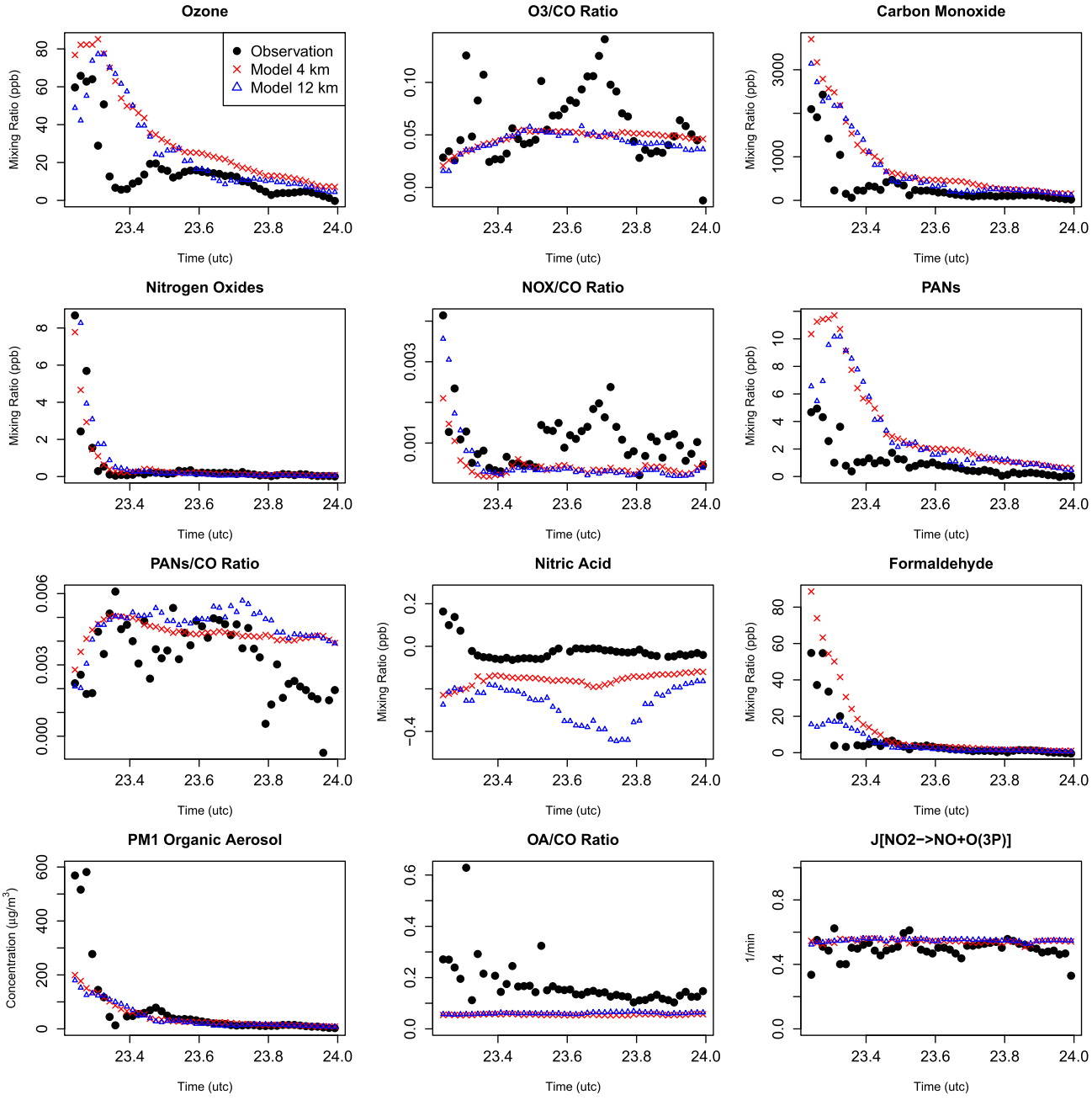

Fig. 4. Measured and modeled comparison of August 26, 2013 centerline plume transect made downwind of the Rim fire (transect as shown in Figs. 3 and S-4). Note that modeled $PM_{2.5}$ organic aerosol is compared to measured PM_1 organic aerosol.

comparable to the model grid resolution. Plume dilution has been identified as an important factor in near-fire production of secondary organic aerosol (Bian et al., 2017) before production and loss of OA becomes similar in plumes further downwind (Bian et al., 2017; Sakamoto et al., 2016). The modeled OA is largely primarily emitted with little traditional semi-volatile SOA formation and no evaporation and recondensation of primary OA, which explains the modest increase over time in simulated OA/CO ratio. However, another contributing factor may be that primary $PM_{2.5}$ emissions are underestimated. An analysis of aircraft in-plume measurements made downwind of multiple large wildfires including the Rim fire in 2013 suggest $PM_{2.5}$ emissions may be under-estimated when using BlueSky based emissions (Liu et al., 2017). A systematic increase in $PM_{2.5}$ emissions would likely result in better plume-top performance for OA, but could negatively impact surface level performance meaning other processes such as vertical distribution of emissions should be considered along with changes in emission factors, treatment of primarily emitted OA as semi-volatile, and effects of horizontal grid resolution.

Particulate sulfate, ammonium, and nitrate ions are generally underestimated at the plume top near the Rim fire (Fig. S-11). These inorganic particulate species have notable gradients between the surface and plume top compared to primarily emitted particulate species suggesting chemical formation is important. Most of the model predicted $PM_{2.5}$ ammonium and nitrate were secondarily formed, although sulfate is largely primarily formed near the fire until secondary production becomes equivalent in terms of total predicted mass further downwind (Fig. S-12). Since very little nitric acid was measured and modeled at the top of the plume, $PM_{2.5}$ nitrate underestimates may be related to underestimated primary emissions. $PM_{2.5}$ sulfate underestimation may be related to underestimated primary emissions or the lack of

hydroxyl radical in the model downwind of the fire (Fig. S-13) inhibiting sulfur dioxide conversion to sulfuric acid since ammonia is abundant in the modeled plume. Underestimated primary emissions of $PM_{2.5}$ sulfate, ammonium, and nitrate could be related to either total emissions or the speciation of those emissions (Table S-4) assumed here.

3.4. Surface comparison

Hourly model predictions of surface level O_3 are compared with measurements from the CASTNET site at Yosemite near the Rim fire in Fig. 5. Model estimates are colored by the percent of the model prediction attributable to emissions from wildfire, where warmer colors represent higher contribution. The modeling system often over-estimates daytime surface level O_3 at this site when the model predicts a large contribution from wildfire. Wild fire emissions appear to destroy (most likely through NO titration) O_3 during nighttime based on the comparison between simulations with and without wild fire emissions. This is most evident in very close proximity to the fire as this feature is only seen at the Yosemite monitor. The modeling system tends to systematically underestimate O_3 at Yosemite on both days with fire and no fire impact, which is likely due to underestimated O_3 inflow to high elevation areas from the global GEOS-CHEM model simulation (Baker et al., 2015).

Modeled Rim fire emissions of $PM_{2.5}$ are dominated by organic aerosol (see Table S-4). Surface level daily average $PM_{2.5}$ organic carbon predictions by the model were paired with daily average ambient measurements taken at IMPROVE monitor locations near the Rim fire in Fig. 6. Even though the modeling system under-estimated $PM_{2.5}$ OA aloft (Fig. 4) and AOD far downwind of the fire (e.g., Fig. 2), estimates of $PM_{2.5}$ organic carbon are generally consistent with measurements at Yosemite (YOSE1), Desolation Wildland Area (BLIS1), and Hoover Wildland Area (HOOV1) (Fig. 6). The largest modeled impacts at Yosemite are in early September and the model does well at representing this period of elevated ambient $PM_{2.5}$ organic carbon. However, the model predicts large O_3 from wild fire at Yosemite during this same time period, while monitored values do not appear either unusually elevated or titrated (Fig. 5). The model over-estimates $PM_{2.5}$ elemental carbon and nitrate ion on days when the model indicates large contribution from the Rim fire and shows little bias on non-fire days (Figs. S-14 and S-15). The surface-level overestimates of $PM_{2.5}$ nitrate ion are in contrast to under-estimates at the plume top discussed previously. Modeled $PM_{2.5}$ sulfate ion compares well with measurements and performance is largely unbiased during periods of Rim fire impacts at these monitors (Fig. S-16). The presence of observed surface level elevated $PM_{2.5}$ due to the Rim fire but not coincident elevated O_3 suggests that $PM_{2.5}$, non-reactive tracers acting like PM, or satellite AOD may not always be a strong indicator for surface level O_3 impacts from wildfire.

Smoke plume interactions with urban pollutant mixtures may result in different outcomes in terms of chemical production of O_3 compared with rural monitors. Coincident surface level measurements of CO, NO_Y, $PM_{2.5}$, and O_3 in Reno, Nevada between 2013 and 2016 suggest elevated ratios of CO:NO_Y are often associated with elevated $PM_{2.5}$ (Fig. 7), which is an indication that a site may be influenced by biomass burning emissions. This relationship is very pronounced during the period of the Rim fire in 2013 (Fig. 8). Periods of biomass burning impacts in Reno between 2013 and 2016 sometimes result in observed O_3 enhancement (Fig. 7), but often do not show pronounced O_3 enhancement which is the case during the Rim fire time period (Fig. 8). Furthermore, there is evidence from studies near O_3 sources that fire emissions positively interfere with UV-absorption measurements of O_3 (Wentworth et al., 2018), but the distance over which such interferences have meaningful impact is not well quantified. It is likely that O_3 is not being formed through the entire boundary layer column and tends to form toward the plume top meaning less O_3 at the surface to impact surface monitors.

Similar to the rural CASTNET sites, the model overestimates O_3 in Reno during the earlier days of the Rim fire (August 22–23) when the model predicts a large contribution from the fire. The model overestimates hourly $PM_{2.5}$ on August 22 but does well capturing the peak on the following day. During the last week of August ambient data shows elevated spikes of hourly $PM_{2.5}$ that are consistent with modeled impacts of the Rim Fire. Only a few days in Reno show elevated O_3 concentrations and these days are well characterized by the model although only one day has model predicted contribution from wild fire exceeding 50% (Fig. 8). The model does well at capturing synoptic patterns in CO and NO_z (sum of all reactive nitrogen oxides excluding NO and NO_2), in Reno. Hourly NO_Y and NO_X is systematically under-predicted by the model with contribution from wildfire routinely exceeding 50% on most hours between August 22 and the end of the month for CO and the oxidized nitrogen gases (Fig. S-17). An increase in measured NO_Z is evident starting on August 21 and decreases in late August, which coincides with the general time period of the Rim fire. The model does well at capturing this broad increase although does not always capture the timing of inflow and outflow on certain days. Some of the discrepancies between modeled estimates and measurements could be partially related to the model representation of winds in complex terrain. Wind speed tends to be over-estimated at the surface, especially for sites at high elevation in the Sierra Nevada (Fig. S-5).

4. Conclusions

The modeling system does well at replicating local to regional scale transport of smoke from large wildfires in California during the 2013 fire season compared to satellite AOD and aircraft transect chemical measurements. Downwind surface $PM_{2.5}$ predicted by the model

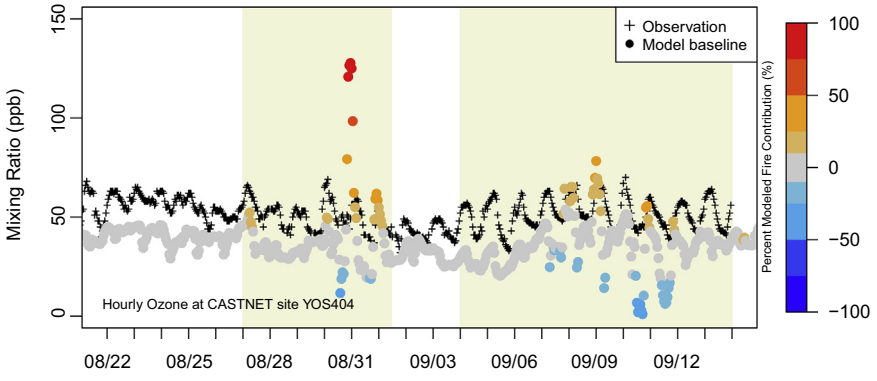

Fig. 5. Surface level O_3 model and monitor comparison at Yosemite National Park where modeled wildland fire contribution to modeled O_3 is shown by color shading. Time periods where impacts from wildland fire are more likely based on HMS satellite smoke maps are highlighted in beige. (For interpretation of the references to color in this figure legend, the reader is referred to the web version of this article.)

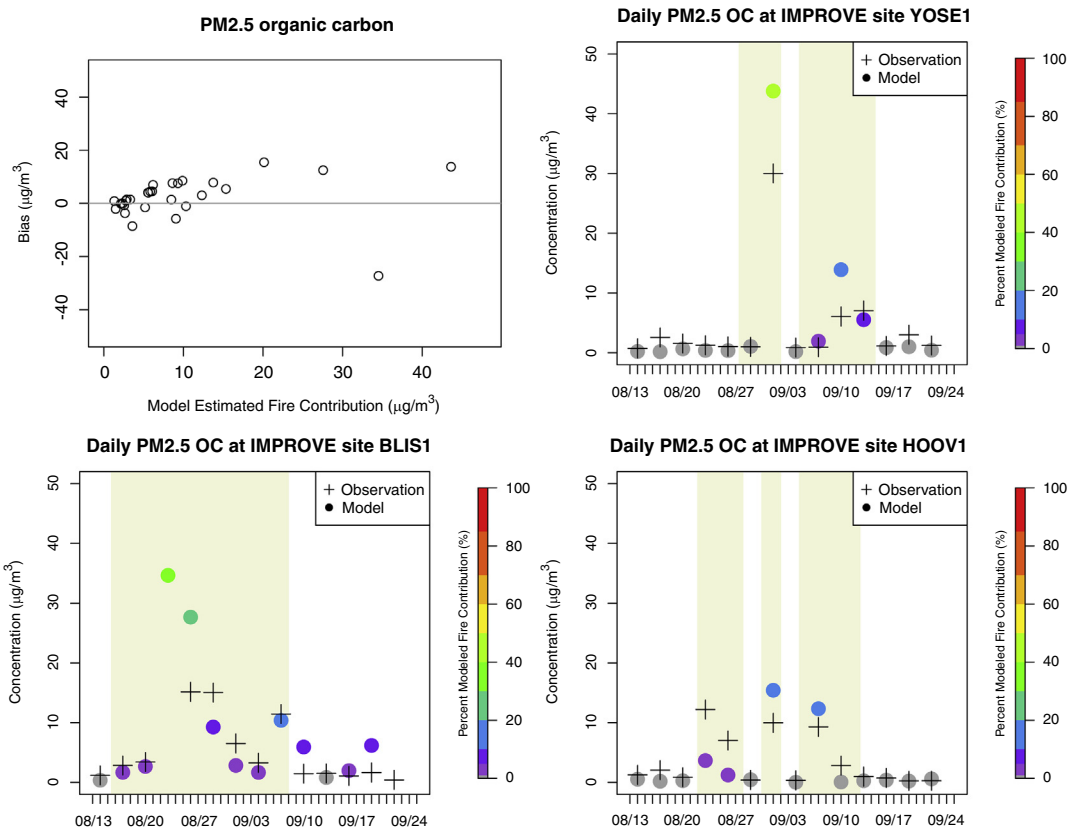

Fig. 6. Daily average modeled fire contribution (where contribution is greater than 20% of bulk model prediction) paired with bulk model $PM_{2.5}$ organic carbon bias at rural IMPROVE monitors (top left). Model and monitor comparisons are provided for Yosemite National Park (YOSE1), Hoover Wildland Area (HOOV1), and Desolation Wildland Area (BLIS1) where wildland fire contribution to modeled $PM_{2.5}$ organic carbon is shown by warmer color shading. Time periods where impacts from wildland fire are more likely based on HMS satellite smoke maps are highlighted in beige. (For interpretation of the references to color in this figure legend, the reader is referred to the web version of this article.)

generally compares well with measurements while O_3 tends to be overestimated both aloft and at the surface when the model predicts impacts from wildfire. More evaluation is needed to better understand aspects of the modeling system that may contribute to O_3 overestimation such as aerosol attenuation of photolysis throughout the smoke plume column, emissions (including fuel mapping, temporal allocation of emissions, and speciation of VOC and NO_X), and vertical mixing in the smoke plume. It is expected that field studies planned for 2018 and 2019 intended to make extensive chemical and physical measurements in downwind plumes of wildfire in the U.S. will provide valuable information toward supporting this type of evaluation and lead to improvements in model formulation.

Acknowledgements

The authors would like to recognize the contributions of James Beidler, Barron Henderson, Allan Beidler, Chris Allen, and Lara Reynolds. Special appreciation for everyone involved in the field study data collection, in particular Thomas Hanisco, John Crounse, Paul Wennberg, Samuel Hall, Greg Huey, Andreas Beyersdorf, Thomas Ryerson, and Armin

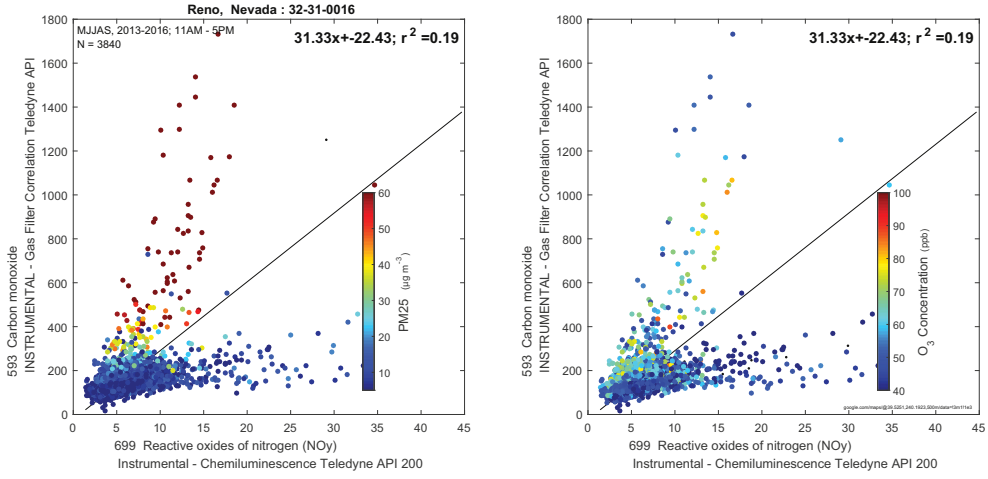

Fig. 7. Hourly comparison of ambient CO and NO_Y at Reno, NV during March through September of 2013 to 2016 shaded by $PM_{2.5}$ (left) and O_3 (right). Only data collected between 11 am and 5 pm are shown. Elevated ratios of $CO:NO_Y$ are often associated with elevated $PM_{2.5}$ but less often with elevated O_3.

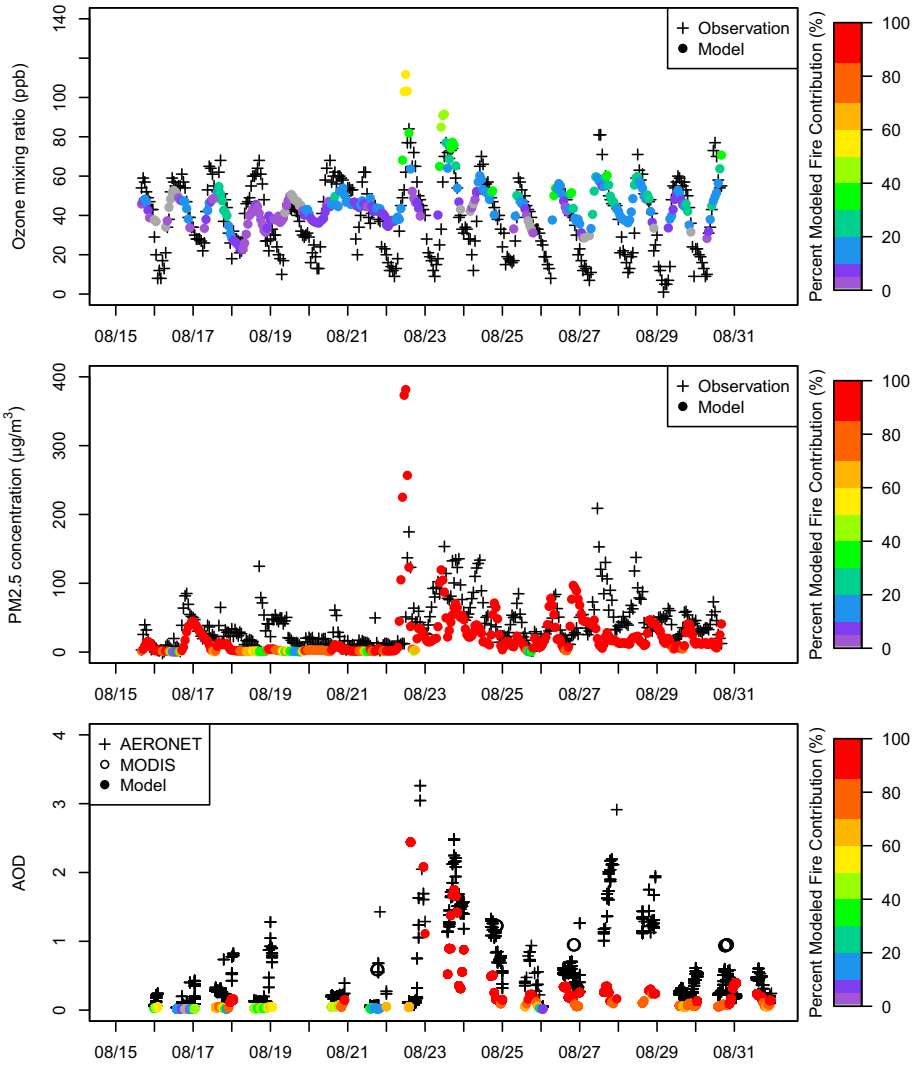

Fig. 8. Model estimates paired with measured O_3 (top) and $PM_{2.5}$ (middle), and AOD at Reno, NV. Wildland fire contribution to modeled values is shown by warmer color shading. (For interpretation of the references to color in this figure legend, the reader is referred to the web version of this article.)

Wisthaler. PCJ and JLJ were supported by NASA NNX15AT96G, and AJS and HDC are supported by NASA NNX16AM30G.

Disclaimer

The views expressed in this article are those of the authors and do not necessarily represent the views or policies of the U.S. Environmental Protection Agency.

Appendix A. Supplementary data

Supplementary data to this article can be found online at https://doi.org/10.1016/j.scitotenv.2018.05.048.

References

Abatzoglou, J.T., Williams, A.P., 2016. Impact of anthropogenic climate change on wildfire across western US forests. Proc. Natl. Acad. Sci. 113, 11770–11775.

Al-Saadi, J., Szykman, J., Pierce, R.B., Kittaka, C., Neil, D., Chu, D.A., Remer, L., Gumley, L., Prins, E., Weinstock, L., 2005. Improving national air quality forecasts with satellite aerosol observations. Bull. Am. Meteorol. Soc. 86, 1249–1261.

Al-Saadi, J., Soja, A.J., Pierce, R.B., Szykman, J., Wiedinmyer, C., Emmons, L., Kondragunta, S., Zhang, X., Kittaka, C., Schaack, T., 2008. Intercomparison of near-real-time biomass burning emissions estimates constrained by satellite fire data. J. Appl. Remote. Sens. 2, 021504–021524.

Baker, K.R., Misenis, C., Obland, M.D., Ferrare, R.A., Scarino, A.J., Kelly, J.T., 2013. Evaluation of surface and upper air fine scale WRF meteorological modeling of the May and June 2010 CalNex period in California. Atmos. Environ. 80, 299–309.

Baker, K.R., Hawkins, A., Kelly, J.T., 2014. Photochemical grid model performance with varying horizontal grid resolution and sub-grid plume treatment for the Martins Creek near-field SO 2 study. Atmos. Environ. 99, 148–158.

Baker, K.R., Emery, C., Dolwick, P., Yarwood, G., 2015. Photochemical grid model estimates of lateral boundary contributions to ozone and particulate matter across the continental United States. Atmos. Environ. 123, 49–62.

Baker, K., Woody, M., Tonnesen, G., Hutzell, W., Pye, H., Beaver, M., Pouliot, G., Pierce, T., 2016. Contribution of regional-scale fire events to ozone and $PM_{2.5}$ air quality estimated by photochemical modeling approaches. Atmos. Environ. 140, 539–554.

Balch, J.K., Bradley, B.A., Abatzoglou, J.T., Nagy, R.C., Fusco, E.J., Mahood, A.L., 2017. Human-started wildfires expand the fire niche across the United States. Proc. Natl. Acad. Sci. 114, 2946–2951.

Bash, J., Baker, K.R., Beaver, M., 2015. Evaluation of improved land use and canopy representation in BEIS v3. 61 with biogenic VOC measurements in California. Geosci. Model Dev. Discuss. 8, 8117–8154.

Bian, Q., Jathar, S.H., Kodros, J.K., Barsanti, K.C., Hatch, L.E., May, A.A., Kreidenweis, S.M., Pierce, J.R., 2017. Secondary organic aerosol formation in biomass-burning plumes: theoretical analysis of lab studies and ambient plumes. Atmos. Chem. Phys. 17, 5459–5475.

Binkowski, F.S., Arunachalam, S., Adelman, Z., Pinto, J.P., 2007. Examining photolysis rates with a prototype online photolysis module in CMAQ. J. Appl. Meteorol. Climatol. 46, 1252–1256.

Boys, B., Martin, R., Van Donkelaar, A., MacDonell, R., Hsu, N., Cooper, M., Yantosca, R., Lu, Z., Streets, D., Zhang, Q., 2014. Fifteen-year global time series of satellite-derived fine particulate matter. Environ. Sci. Technol. 48, 11109–11118.

Cai, C., Kulkarni, S., Zhao, Z., Kaduwela, A.P., Avise, J.C., DaMassa, J.A., Singh, H.B., Weinheimer, A.J., Cohen, R.C., Diskin, G.S., 2016. Simulating reactive nitrogen, carbon monoxide, and ozone in California during ARCTAS-CARB 2008 with high wildfire activity. Atmos. Environ. 128, 28–44.

CAL FIRE, 2013. American Fire Incident Information. http://cdfdata.fire.ca.gov/incidents/incidents_details_info?incident_id=877, Accessed date: 10 February 2018.
Carlton, A.G., Bhave, P.V., Napelenok, S.L., Edney, E.O., Sarwar, G., Pinder, R.W., Pouliot, G.A., Houyoux, M., 2010. Treatment of secondary organic aerosol in CMAQv4.7. Environ. Sci. Technol. 44, 8553–8560.
Cubison, M., Ortega, A., Hayes, P., Farmer, D., Day, D., Lechner, M., Brune, W., Apel, E., Diskin, G., Fisher, J., 2011. Effects of aging on organic aerosol from open biomass burning smoke in aircraft and laboratory studies. Atmos. Chem. Phys. 11, 12049–12064.
DeCarlo, P.F., Kimmel, J.R., Trimborn, A., Northway, M.J., Jayne, J.T., Aiken, A.C., Gonin, M., Fuhrer, K., Horvath, T., Docherty, K.S., 2006. Field-deployable, high-resolution, time-of-flight aerosol mass spectrometer. Anal. Chem. 78, 8281–8289.
Dunlea, E., DeCarlo, P., Aiken, A., Kimmel, J., Peltier, R., Weber, R., Tomlinson, J., Collins, D.R., Shinozuka, Y., McNaughton, C., 2009. Evolution of Asian aerosols during transpacific transport in INTEX-B. Atmos. Chem. Phys. 9, 7257–7287.
Emery, C., Jung, J., Koo, B., Yarwood, G., 2015. Improvements to CAMx Snow Cover Treatments and Carbon Bond Chemical Mechanism for Winter Ozone. Prepared for the Utah Department of Environmental Quality. Division of Air Quality, Salt Lake City, UT Available at:. http://www.camx.com/files/udaq_snowchem_final_6aug15.pdf.
Fahey, K.M., Carlton, A.G., Pye, H.O., Baek, J., Hutzell, W.T., Stanier, C.O., Baker, K.R., Appel, K.W., Jaoui, M., Offenberg, J.H., 2017. A framework for expanding aqueous chemistry in the Community Multiscale Air Quality (CMAQ) model version 5.1. Geosci. Model Dev. 10.
Fann, N., Fulcher, C.M., Baker, K., 2013. The recent and future health burden of air pollution apportioned across US sectors. Environ. Sci. Technol. 47, 3580–3589.
Fisher, J.A., Jacob, D.J., Travis, K.R., Kim, P.S., Marais, E.A., Chan Miller, C., Yu, K., Zhu, L., Yantosca, R.M., Sulprizio, M.P., 2016. Organic nitrate chemistry and its implications for nitrogen budgets in an isoprene-and monoterpene-rich atmosphere: constraints from aircraft (SEAC 4 RS) and ground-based (SOAS) observations in the Southeast US. Atmos. Chem. Phys. 16, 5969–5991.
Forrister, H., Liu, J., Scheuer, E., Dibb, J., Ziemba, L., Thornhill, K.L., Anderson, B., Diskin, G., Perring, A.E., Schwarz, J.P., 2015. Evolution of Brown carbon in wildfire plumes. Geophys. Res. Lett. 42 (11), 4623–4630.
Fountoukis, C., Nenes, A., 2007. ISORROPIA II: a computationally efficient thermodynamic equilibrium model for K+-Ca2+-Mg2+-Nh(4)(+)-Na+-SO42–NO3–Cl–H2O aerosols. Atmos. Chem. Phys. 7, 4639–4659.
Hair, J.W., Hostetler, C.A., Cook, A.L., Harper, D.B., Ferrare, R.A., Mack, T.L., Welch, W., Izquierdo, L.R., Hovis, F.E., 2008. Airborne high spectral resolution lidar for profiling aerosol optical properties. Appl. Opt. 47, 6734–6752.
Hao, W.M., Larkin, N.K., 2014. Wildland fire emissions, carbon, and climate: wildland fire detection and burned area in the United States. For. Ecol. Manag. 317, 20–25.
Henderson, B., Akhtar, F., Pye, H., Napelenok, S., Hutzell, W., 2014. A database and tool for boundary conditions for regional air quality modeling: description and evaluation. Geosci. Model Dev. 7, 339–360.
Kaufman, Y., Tanré, D., Remer, L.A., Vermote, E., Chu, A., Holben, B., 1997. Operational remote sensing of tropospheric aerosol over land from EOS moderate resolution imaging spectroradiometer. J. Geophys. Res.-Atmos. 102, 17051–17067.
Kondragunta, S., Lee, P., McQueen, J., Kittaka, C., Prados, A., Ciren, P., Laszlo, I., Pierce, R., Hoff, R., Szykman, J., 2008. Air quality forecast verification using satellite data. J. Appl. Meteorol. Climatol. 47, 425–442.
Kwok, R., Napelenok, S., Baker, K., 2013. Implementation and evaluation of $PM_{2.5}$ source contribution analysis in a photochemical model. Atmos. Environ. 80, 398–407.
Kwok, R., Baker, K., Napelenok, S., Tonnesen, G., 2015. Photochemical grid model implementation of VOC, NOx, and O_3 source apportionment. Geosci. Model Dev. 8, 99–114.
Larkin, N.K., O'Neill, S.M., Solomon, R., Raffuse, S., Strand, T., Sullivan, D.C., Krull, C., Rorig, M., Peterson, J., Ferguson, S.A., 2010. The BlueSky smoke modeling framework. Int. J. Wildland Fire 18, 906–920.
Levy, R., Mattoo, S., Munchak, L., Remer, L., Sayer, A., Patadia, F., Hsu, N., 2013. The collection 6 MODIS aerosol products over land and ocean. Atmospheric Measurement Techniques 6, 2989.
Liu, J.C., Pereira, G., Uhl, S.A., Bravo, M.A., Bell, M.L., 2015. A systematic review of the physical health impacts from non-occupational exposure to wildfire smoke. Environ. Res. 136, 120–132.
Liu, X., Zhang, Y., Huey, L., Yokelson, R., Wang, Y., Jimenez, J., Campuzano-Jost, P., Beyersdorf, A., Blake, D., Choi, Y., 2016a. Agricultural fires in the southeastern US during SEAC4RS: emissions of trace gases and particles and evolution of ozone, reactive nitrogen, and organic aerosol. J. Geophys. Res.-Atmos. 121, 7383–7414.
Liu, Z., Murphy, J.P., Maghirang, R., Devlin, D., 2016b. Health and environmental impacts of smoke from vegetation fires: a review. J. Environ. Prot. 7, 1860–1885.
Liu, X., Huey, L.G., Yokelson, R.J., Selimovic, V., Simpson, I.J., Müller, M., Jimenez, J.L., Campuzano-Jost, P., Beyersdorf, A.J., Blake, D.R., Butterfield, Z., Choi, Y., Crounse, J.D., Day, D.A., Diskin, G.S., Dubey, M.K., Fortner, E., Hanisco, T.F., Hu, W., King, L.E., Kleinman, L., Meinardi, S., Mikoviny, T., Onasch, T.B., Palm, B.B., Peischl, J., Pollack, I.B., Ryerson, T.B., Sachse, G.W., Sedlacek, A.J., Shilling, J.E., Springston, S., St. Clair, J.M., Tanner, D.J., Teng, A.P., Wennberg, P.O., Wisthaler, A., Wolfe, G.M., 2017. Airborne measurements of western U.S. wildfire emissions: comparison with prescribed burning and air quality implications. J. Geophys. Res.-Atmos. 122 (11), 6108–6129.
Loría-Salazar, S.M., Holmes, H.A., Arnott, W.P., Barnard, J.C., Moosmüller, H., 2016. Evaluation of MODIS columnar aerosol retrievals using AERONET in semi-arid Nevada and California, USA, during the summer of 2012. Atmos. Environ. 144, 345–360.
McKeen, S., Wotawa, G., Parrish, D., Holloway, J., Buhr, M., Hübler, G., Fehsenfeld, F., Meagher, J., 2002. Ozone production from Canadian wildfires during June and July of 1995. J. Geophys. Res.-Atmos. 107.
Molod, A., Takacs, L., Suarez, M., Bacmeister, J., 2015. Development of the GEOS-5 atmospheric general circulation model: evolution from MERRA to MERRA2. Geosci. Model Dev. 8, 1339.
Munchak, L., Levy, R., Mattoo, S., Remer, L., Holben, B., Schafer, J., Hostetler, C., Ferrare, R., 2013. MODIS 3 km Aerosol Product: Applications Over Land in an Urban/Suburban Region.
Omar, A.H., Winker, D.M., Vaughan, M.A., Hu, Y., Trepte, C.R., Ferrare, R.A., Lee, K.-P., Hostetler, C.A., Kittaka, C., Rogers, R.R., 2009. The CALIPSO automated aerosol classification and lidar ratio selection algorithm. J. Atmos. Ocean. Technol. 26, 1994–2014.
Peterson, D.A., Hyer, E.J., Campbell, J.R., Fromm, M.D., Hair, J.W., Butler, C.F., Fenn, M.A., 2015. The 2013 rim fire: implications for predicting extreme fire spread, pyroconvection, and smoke emissions. Bull. Am. Meteorol. Soc. 96, 229–247.
Pitchford, M., Malm, W., Schichtel, B., Kumar, N., Lowenthal, D., Hand, J., 2007. Revised algorithm for estimating light extinction from IMPROVE particle speciation data. J. Air Waste Manage. Assoc. 57, 1326–1336.
Raffuse, S., Pryden, D.A., Sullivan, D.C., Larkin, N.K., Strand, T., Solomon, R., 2009. SMARTFIRE Algorithm Description, Sonoma Tech Memo STI-905517-3719, Prepared for U.S. Environmental Protection Agency by Sonoma Technology, Inc., 2009.
Rappold, A.G., Stone, S.L., Cascio, W.E., Neas, L.M., Kilaru, V.J., Sue Carraway, M., Szykman, J.J., Ising, A., Cleve, W.E., Meredith, J.T., 2011. Peat bog wildfire smoke exposure in rural North Carolina is associated with cardiopulmonary emergency department visits assessed through syndromic surveillance. Environ. Health Perspect. 119, 1415.
Reid, J.S., Hyer, E.J., Prins, E.M., Westphal, D.L., Zhang, J., Wang, J., Christopher, S.A., Curtis, C.A., Schmidt, C.C., Eleuterio, D.P., 2009. Global monitoring and forecasting of biomass-burning smoke: description of and lessons from the fire locating and modeling of burning emissions (FLAMBE) program. IEEE J. Sel. Top. Appl. Earth Obs. Remote Sens. 2, 144–162.
Reid, C.E., Brauer, M., Johnston, F.H., Jerrett, M., Balmes, J.R., Elliott, C.T., 2016. Critical review of health impacts of wildfire smoke exposure. Environ. Health Perspect. 124, 1334.
Rolph, G.D., Draxler, R.R., Stein, A.F., Taylor, A., Ruminski, M.G., Kondragunta, S., Zeng, J., Huang, H.-C., Manikin, G., McQueen, J.T., 2009. Description and verification of the NOAA smoke forecasting system: the 2007 fire season. Weather Forecast. 24, 361–378.
Saide, P.E., Peterson, D.A., Silva, A., Anderson, B., Ziemba, L.D., Diskin, G., Sachse, G., Hair, J., Butler, C., Fenn, M., 2015. Revealing important nocturnal and day-to-day variations in fire smoke emissions through a multiplatform inversion. Geophys. Res. Lett. 42, 3609–3618.
Sakamoto, K.M., Laing, J.R., Stevens, R.G., Jaffe, D.A., Pierce, J.R., 2016. The evolution of biomass-burning aerosol size distributions due to coagulation: dependence on fire and meteorological details and parameterization. Atmos. Chem. Phys. 16, 7709–7724.
Schoennagel, T., Balch, J.K., Brenkert-Smith, H., Dennison, P.E., Harvey, B.J., Krawchuk, M.A., Mietkiewicz, N., Morgan, P., Moritz, M.A., Rasker, R., 2017. Adapt to more wildfire in western North American forests as climate changes. Proc. Natl. Acad. Sci. 114, 4582–4590.
Shrivastava, M., Cappa, C.D., Fan, J., Goldstein, A.H., Guenther, A.B., Jimenez, J.L., Kuang, C., Laskin, A., Martin, S.T., Ng, N.L., 2017. Recent advances in understanding secondary organic aerosol: implications for global climate forcing. Rev. Geophys. 55 (2), 509–559.
Sicard, M., Pérez, C., Rocadenbosch, F., Baldasano, J., García-Vizcaino, D., 2006. Mixed-layer depth determination in the Barcelona coastal area from regular lidar measurements: methods, results and limitations. Bound.-Layer Meteorol. 119, 135–157.
Simon, H., Bhave, P.V., 2012. Simulating the degree of oxidation in atmospheric organic particles. Environ. Sci. Technol. 46, 331–339.
Simpson, I.J., Akagi, S., Barletta, B., Blake, N., Choi, Y., Diskin, G., Fried, A., Fuelberg, H., Meinardi, S., Rowland, F., 2011. Boreal forest fire emissions in fresh Canadian smoke plumes: C 1-C 10 volatile organic compounds (VOCs), CO 2, CO, NO 2, NO, HCN and CH 3 CN. Atmos. Chem. Phys. 11, 6445–6463.
Skamarock, W.C., Klemp, J.B., Dudhia, J., Gill, D.O., Barker, D.M., Duda, M.G., Huang, X., Wang, W., Powers, J.G., 2008. A Description of the Advanced Reserch WRF Version 3. NCAR Technical Note NCAR/TN-475+STR.
Soja, A., Fairlie, T., Westberg, D., Pouliot, G., 2012. Biomass burning plume injection height using CALIOP, MODIS and the NASA Langley Trajectory Model. 2012 International Emission Inventory Conference https://www3.epa.gov/ttnchie1/conference/ei20/session7/asoja.pdf.
Tanré, D., Kaufman, Y., Herman, M., Mattoo, S., 1997. Remote sensing of aerosol properties over oceans using the MODIS/EOS spectral radiances. J. Geophys. Res.-Atmos. 102, 16971–16988.
Toon, O.B., Maring, H., Dibb, J., Ferrare, R., Jacob, D.J., Jensen, E.J., Luo, Z.J., Mace, G.G., Pan, L.L., Pfister, L., 2016. Planning, implementation, and scientific goals of the studies of emissions and atmospheric composition, clouds and climate coupling by regional surveys (SEAC4RS) field mission. J. Geophys. Res.-Atmos. 121, 4967–5009.
Urbanski, S., 2013. Combustion efficiency and emission factors for wildfire-season fires in mixed conifer forests of the northern Rocky Mountains, US. Atmos. Chem. Phys. 13, 7241–7262.
Van Donkelaar, A., Martin, R.V., Park, R.J., 2006. Estimating ground-level $PM_{2.5}$ using aerosol optical depth determined from satellite remote sensing. J. Geophys. Res.-Atmos. 111.
Van Donkelaar, A., Martin, R.V., Brauer, M., Hsu, N.C., Kahn, R.A., Levy, R.C., Lyapustin, A., Sayer, A.M., Winker, D.M., 2016. Global estimates of fine particulate matter using a combined geophysical-statistical method with information from satellites, models, and monitors. Environ. Sci. Technol. 50, 3762–3772.
Wagstrom, K.M., Baker, K.R., Leinbach, A.E., Hunt, S.W., 2014. Synthesizing scientific progress: Outcomes from US EPA's carbonaceous aerosols and source apportionment STAR grants. Environ. Sci. Technol. 48, 10561–10570.
Wentworth, G.R., Aklilu, Y.-A., Landis, M.S., Hsu, Y.-M., 2018. Impacts of a large boreal wildfire on ground level atmospheric concentrations of PAHs, VOCs and ozone. Atmos. Environ. 178, 19–30.

Yates, E., Iraci, L., Singh, H., Tanaka, T., Roby, M., Hamill, P., Clements, C., Lareau, N., Contezac, J., Blake, D., 2016. Airborne measurements and emission estimates of greenhouse gases and other trace constituents from the 2013 California Yosemite Rim wildfire. Atmos. Environ. 127, 293–302.

Yu, P., Toon, O.B., Bardeen, C.G., Bucholtz, A., Rosenlof, K.H., Saide, P.E., Da Silva, A., Ziemba, L.D., Thornhill, K.L., Jimenez, J.L., 2016. Surface dimming by the 2013 rim fire simulated by a sectional aerosol model. J. Geophys. Res.-Atmos. 121, 7079–7087.

Zhou, L., Baker, K.R., Napelenok, S.L., Pouliot, G., Elleman, R., O'Neill, S.M., Urbanski, S.P., Wong, D.C., 2018. Modeling crop residue burning experiments to evaluate smoke emissions and plume transport. Sci. Total Environ. 627, 523–533.

Zoogman, P., Jacob, D.J., Chance, K., Liu, X., Lin, M., Fiore, A., Travis, K., 2014. Monitoring high-ozone events in the US intermountain west using TEMPO geostationary satellite observations. Atmos. Chem. Phys. 14, 6261–6271.